Hindawi
Journal of Sensors
Volume 2022, Article ID 6554128, 19 pages
https://doi.org/10.1155/2022/6554128

Research Article

The Effect of Bit Depth on High-Temperature Digital Image Correlation Measurements

Steven R. Jarrett,[1] Thinh Q. Thai,[2] Lindsey J. Rowley,[1] Weston D. Craig,[1] and Ryan B. Berke[1]

[1]*Utah State University, Mechanical and Aerospace Engineering, 4130 Old Main Hill, Logan, UT 84322, USA*
[2]*Van Lang University, Faculty of Mechanical-Electrical, and Computer Engineering, 69/68 Dang Thuy Tram Street, Ward 13, Binh Thanh District, Ho Chi Minh City, Vietnam*

Correspondence should be addressed to Ryan B. Berke; ryan.berke@usu.edu

Received 31 March 2022; Accepted 3 May 2022; Published 2 June 2022

Academic Editor: Carlos Marques

Digital Image Correlation (DIC) is a camera-based method of measuring displacement and strain. High-temperature DIC is challenging due to light emitted from the sample which can saturate the image. This effect can be mitigated using optical bandpass filters, but the maximum sample temperature range of DIC remains dependent on the camera and camera settings. Among camera settings, bit depth, also referred to as color depth or number of bits, has received insufficient attention in high-temperature DIC literature. In this work, the effect of bit depth on DIC measurements is investigated both analytically and experimentally. It is shown that if image noise is sufficiently low, then increasing bit depth reduces DIC random error. A new metric, the effective number of bits, is presented to determine the appropriate number of bits for DIC images. Using increased bit depth, reduced exposure time, and low-noise images, the maximum sample temperature for DIC measurements was shown to increase without negatively impacting random error.

1. Introduction

Digital Image Correlation (DIC) is a camera-based method of measuring displacement and strain. Since its first practical application in the 1980s [1], popularity of the technique in peer-reviewed literature has grown exponentially while other popular strain-measurement methods have not seen a significant increase in use [2]. One area of current research is in increasing the range of sample temperatures for which DIC can be used. The purpose of this work is to explore the effect of a camera's bit depth, also referred to as color depth or number of bits, on the resulting DIC measurement in an effort to increase this range of temperatures.

Performing DIC on high-temperature samples can be challenging due to light emitted from the sample according to Planck's law [3]. Because images of the sample include both reflected and emitted light, then as sample temperature and emitted light increase, the image brightens until eventually there is saturation of the camera sensor. At relatively low temperatures, this is not a problem because emitted light is not a significant portion of the light collected by the sensor. In situations where the amount of emitted light is significant and sample temperature may change over the course of the experiment, the user must be careful to select a correlation function which corrects for this type of change in lighting [4]. As early as 1996, Lyons et al. demonstrated DIC to be capable of measuring samples at temperatures up to 650°C [5].

Because the emitted light is known to be brighter at longer wavelengths [6], one solution to the background radiation problem is to use a blue (~450 nm) light source and bandpass optical filter. In 2009, Grant et al. showed that using blue-light illumination and optical filtering could extend the maximum temperature of DIC measurements to at least 1000°C [7]. Two years later, this was extended to 1500°C by Novak and Zok [8] and has been used in several other high-temperature experiments [9–15]. Most recently, the temperature limit of blue-DIC has been extended to

3067°C by Pan et al. [9]. In their work, the authors utilized the difference in the spectral emissivity of tantalum carbide and tungsten to create a speckle pattern that would work at any temperature. As the temperature increased, however, the authors were forced to adjust the lighting conditions and exposure time between three discrete temperature intervals, which increases DIC measurement uncertainty [9, 16].

The idea of using an optical filter has also been extended to shorter wavelengths, primarily in the UV range. In 2014, Berke and Lambros took the idea of blue-DIC further by using ultraviolet (UV) lighting and a UV bandpass filter to further reduce background radiation from the sample in 2D-DIC images [17]. This idea was later demonstrated successfully with 3D UV-DIC by Dong and Pan in 2019 [18]. Other variations of UV-DIC include ultraviolet diffraction-assisted image correlation (UV-DAIC) for taking 3D measurements with a single camera [19] and high-magnification UV-DIC at long working distances [20]. In spite of the use of optical filters, however, DIC images still suffer from offsets in lighting at extreme temperatures, requiring the user to balance the risk of overexposure with the risk of not having enough contrast for effective DIC measurement [6]. This might be mitigated by continuing to shorten the wavelength of the light source and filter, but doing so increases the radiation health risk to the user. At one extreme, Jones et al. recently used X-ray-based DIC to overcome warping of the air due to combined heat haze and shock wave conditions [21].

Because it is impossible to filter out all thermal radiation from high-temperature specimens, the maximum sample temperature of DIC also depends on the camera and camera settings. In an effort to quantify the relationship between camera settings and maximum temperature, Thai et al. published a series of articles where he correlated images of a high-temperature specimen taken at multiple temperatures and exposure times and analyzed the effect of exposure time [6, 16, 22], temperature [22, 23], and the correlation criterion [4, 22] on both the images and the resulting DIC random error. In his work, Thai pointed out that increases in sample temperature tend to produce offsets in sample lighting whereas changes in camera sensitivity (such as exposure time) produce linear scaling in lighting. His article concludes by suggesting a normalized metric, Δ, representing the range of the median 90% of all pixel values which should be minimized but kept above a minimum of 50 (for an 8-bit camera) for effective DIC measurements at high temperatures. Thai's suggestion builds on two similar recommendations: the first, made by Reu [24], that the difference in intensity between "typical" bright and dark pixels should be at least 50 grayscale values (counts), and the second, made by the International Digital Image Correlation Society (iDICs) [25], that the contrast should be at least 20% for an 8-bit camera.

One way to increase Δ is by increasing bit depth. However, whether or not increasing bit depth improves high-temperature DIC measurements has not yet been explored in high-temperature DIC literature. The purpose of this work is to explore the effect of bit depth on both the random error and the maximum sample temperature of DIC measurements. First, a theoretical foundation is established including a discussion of the effect of bit depth on DIC uncertainty. Then, a preliminary noise study is conducted to compare the uncertainty of 8-bit and 12-bit DIC displacement measurements as a function of image noise. Then, a series of room temperature experiments explore the effect of exposure time on DIC measurements for multiple bit depths and levels of image noise. Finally, the room temperature experiments are repeated as a function of temperature. It is shown that, for relatively low-noise images, higher bit depth can improve high-temperature DIC measurements through reduced uncertainty and/or the ability to select modestly shorter exposure times; but for relatively high-noise images, higher bit depth shows no meaningful improvement over 8-bit images.

2. Theory

To establish a theoretical foundation for the analysis of the effect of bit depth on DIC measurement uncertainty, it is necessary to first recall a few equations related to image contrast and noise. After the presentation of these below, a few quantitative relationships are then derived as applied to DIC, the theoretical effect of bit depth on DIC measurements is discussed, and the theoretical effect of image averaging is set forth.

2.1. Contrast Metrics for DIC. Before diving into a discussion of the effect of bit depth on DIC, it is necessary to recall a few metrics of image contrast. The Δ metric was created by Thai et al. using an 8-bit camera as a standardized way to measure the contrast between a 'typical' dark pixel and a 'typical' bright pixel in a grayscale image [6]. Equation (1) is the equation for Δ, where Z_1 and Z_2 are the intensity values at which the cumulative distribution function (CDF) of the image equals 0.05 and 0.95, respectively.

$$\Delta = Z_2 - Z_1. \tag{1}$$

The mean intensity gradient (MIG), which was derived by Pan et al. in [26], is another common metric of contrast in an image. The equation for MIG is given in

$$\text{MIG} = \frac{1}{WH}\sum_{i=1}^{W}\sum_{j=1}^{H}\sqrt{I_x(i,j)^2 + I_y(i,j)^2}, \tag{2}$$

where I_x and I_y are the partial derivatives of the image in the horizontal and vertical directions, respectively, where (i, j) denotes a single pixel within the image (counts/pixel), and W and H are the width and height of the image, respectively (pixels).

For DIC measurements, it is typically recommended to maximize contrast in order to minimize DIC errors. However, as discussed in Introduction, this is difficult at high temperatures due to the risk of saturating the camera sensor, which leads to the present discussion of minimizing initial brightness (which reduces contrast) while maintaining sufficient contrast to ensure sufficiently low DIC uncertainty.

2.2. Quantization and Its Effect on Image Noise. Drawing upon work by previous authors, one can determine the relationship between bit depth and DIC displacement uncertainty beginning with a basic understanding of quantization and its contribution to image noise. After light is recorded by the sensor of a digital camera, it is quantized or converted to a discrete value represented using a number of bits. The number of bits is referred to as bit depth. The maximum number of distinct values storable by a B-bit number is 2^B. When the number of bits is changed, the number representing the amount of light incident on a pixel typically scales with the maximum value $(2^B - 1)$ even though the amount of light does not change. This conversion to a discrete value inherently introduces noise [27]. In this work, noise (normally calculated using mean-squared error) is assumed equal to variance, which is true if the noise has zero bias [28].

Image noise (σ_{img}^2) can be expressed as the sum of many smaller contributors, each representing a step in the conversion from an image incident on the sensor to the camera's digital output, as shown in Equation (3); for convenience, quantization noise—the portion of noise which has a unique relationship with bit depth—is separated from other noise sources in the equation.

$$\sigma_{img}^2 = \sigma_Q^2 + \sum_i \sigma_i^2, \tag{3}$$

where σ_{img}^2 is the pixel intensity noise (variance), σ_Q^2 is the quantization noise, and σ_i^2 is all other sources of noise in the system.

Working in units of counts, quantization noise is calculated by representing the error between the quantized value and the true value as a random variable with uniform probability distribution [27] on the interval [-0.5,0.5). Thus, the variance [29] is given by

$$\sigma_Q^2 = \frac{(b-a)^2}{12} = \frac{1}{12}, \tag{4}$$

where $a, b = -0.5, 0.5$ (the lower and upper bounds of quantization error, respectively).

For further elaboration on the source of the 1/12 term, the reader is encouraged to work through Eq. (5.4.4) of [29]. Equation (4) shows that, when working in units of counts, quantization noise is constant regardless of bit depth, camera, temperature, or any other variable. In contrast, noise sources which occur prior to quantization scale with $(2^B - 1)$. Noise sources which occur after quantization (i.e., due to post processing) are neglected for this derivation. Substituting Equation (4) into Equation (3), the total image noise becomes

$$\sigma_{img}^2 = \frac{1}{12} + \sum_i \sigma_i^2. \tag{5}$$

For this work, it was necessary to determine image noise experimentally. Because an image is a collection of pixels, this required obtaining an average of the uncertainty of all pixels within the image. Equation (6) was the equation used for this purpose, which is essentially the mean of the variance of all pixels within the image.

$$\sigma_{img}^2 = \bar{\sigma_I^2} = \frac{1}{HW} \sum_{i=1}^{H} \sum_{j=1}^{W} (\sigma_I(i,j))^2, \tag{6}$$

where $\sigma_I(i,j)$ is the standard deviation of each pixel computed across all images.

Further justification for Equation (6) is given in the appendix of the thesis version of this work [30].

2.3. The Effective Number of Bits (B_{eff}) Metric for Digital Images. One metric related to noise that is used in signal processing is the effective number of bits (B_{eff}) of a system [27]. The metric is typically used to determine the appropriate number of bits used for an analog-to-digital converter, and as shown hereafter, it can similarly be used in DIC experiments to determine the appropriate number of bits to use for image acquisition. This metric has been solved previously for signal-processing and signal-generating systems (see ENOB in [27]) but must be rederived for imaging systems because the underlying assumptions are not the same (the input signal does not vary sinusoidally in a camera). Deriving B_{eff} begins with a definition of the signal-to-quantization-noise ratio (SQNR):

$$\text{SQNR} = \frac{\mu^2}{\sigma_Q^2}, \tag{7}$$

where μ is the mean intensity of a single pixel. This quantity can be rewritten in terms of the number of bits, B, where μ_0 is a bit depth independent measure of the mean ($\mu_0 \in [0, 1]$):

$$\mu = \left(2^B - 1\right)\mu_0. \tag{8}$$

Substituting the known value of 1/12 for σ_Q yields:

$$\text{SQNR} = \left(\sqrt{12} \cdot \left(2^B - 1\right)\mu_0\right)^2. \tag{9}$$

This can be rearranged to solve for B:

$$B = \log_2\left(\frac{\sqrt{\text{SQNR}}}{\sqrt{12} \cdot \mu_0} + 1\right). \tag{10}$$

Equation (10) represents the number of bits used for quantization given a bit-depth-normalized mean (μ_0) and the SQNR. The effective number of bits, then, is what results from Equation (10) if the signal-to-noise ratio ($\text{SNR} = \mu^2/\sigma_{img}^2$, where σ_{img}^2 includes all sources of noise,

not just quantization) is used instead of the SQNR. Substituting and simplifying yields

$$B_{\text{eff}} = \log_2\left(\frac{\sqrt{\text{SNR}}}{\sqrt{12}\cdot\mu_0} + 1\right) = \log_2\left(2^B + \sigma_{img}\sqrt{12} - 1\right) - \log_2\left(\sigma_{img}\sqrt{12}\right). \tag{11}$$

If σ is very small compared to 2^B, then $\sigma_{img}\sqrt{12} - 1$ becomes negligible, and B_{eff} simplifies further to

$$B_{\text{eff}} \approx B - \log_2\left(\sigma_{img}\right) - 1.79. \tag{12}$$

It should be noted that if the only significant noise source present is quantization noise, then $\sigma_{img} = \sigma_Q = 1/\sqrt{12}$, and Equation (12) becomes $B_{\text{eff}} = B$. B_{eff} represents a simple metric which can be used to evaluate the quality of an image in terms of bits, which can then be used to optimize the number of bits used for recording images.

2.4. The Relationship between DIC Displacement Variance and Bit Depth. Image noise contributes to DIC measurement error. In 2009, Wang et al. [31] derived an expression showing the relationship between image noise, the sum of squared differences of intensity between two adjacent subsets, and the variance of a DIC displacement measurement. In one dimension, this relationship is given by

$$\sigma^2_{\text{DIC}} \approx \frac{2\sigma^2_{img}}{\sum_{i=1}^{\text{SS}}\sum_{j=1}^{\text{SS}} I^*_x(i,j)^2}, \tag{13}$$

where σ^2_{DIC} is the variance of DIC displacement (pixels^2); σ^2_{img} is the variance of pixel intensity or image noise (counts^2); SS is the width of a square (SS × SS) subset I^* (pixels); $I^*(i,j)$ is the subset to be correlated, with coordinates (i,j) denoting a specific pixel in I^*; and $I^*_x(i,j) = d/dx(I^*(i,j))$, where x is the direction of interest.

Pan et al. [26] showed that MIG and subset size (SS) can be substituted into the denominator of Equation (13) to estimate DIC uncertainty across an entire image rather than a single subset:

$$\sum_{i=1}^{\text{SS}}\sum_{j=1}^{\text{SS}} I^*_x(i,j)^2 \approx (\text{SS}\cdot\text{MIG})^2, \tag{14}$$

$$\sigma^2_{\text{DIC}} \approx \frac{2\sigma^2_{img}}{\sum_{i=1}^{\text{SS}}\sum_{j=1}^{\text{SS}} I^*_x(i,j)^2} \approx \frac{2\sigma^2_{img}}{\text{SS}^2\text{MIG}^2}. \tag{15}$$

Combining Equations (15) and (5) yields Equation (16), a relationship between DIC variance, image noise (divided into quantization noise and noise from other sources), subset size, and the MIG of the image.

$$\sigma^2_{\text{DIC}} \approx \frac{2\sigma^2_{img}}{\text{SS}^2(\text{MIG})^2} \approx \frac{2\left(1/12 + \sum\sigma_i^2\right)}{\text{SS}^2(\text{MIG})^2}. \tag{16}$$

By examining Equation (16), it is possible to determine the theoretical relationship between bit depth and DIC displacement uncertainty. In the equation, first note that both σ_i and MIG are dependent on the camera/image and thus will scale in proportion to $(2^B - 1)$. As such, an increase in bit depth, B, will increase both terms by the same factor. In contrast, the quantization noise term (1/12) is constant. This means an increase in bit depth will increase both the numerator and the denominator in Equation (15), but the denominator will increase more quickly than the numerator resulting in an overall decrease in DIC variance. Thus, increasing bit depth reduces DIC uncertainty. Although this will always be true mathematically, the reduction is expected to be significant only if the noise from other sources is of similar or smaller magnitude than the noise due to quantization ($\sum\sigma_i^2 \le 1/12$).

2.5. The Effect of Image Averaging. Image averaging is used in this work to control the apparent noise in an image. In theory, the expected noise in an integer-valued averaged image is given by Equation (17), which is based on the equation to find the uncertainty of the mean of multiple measurements [28]. In the equation, the noise in the nonaveraged image is reduced in the averaged image by a factor of N_{avgd}, the number of images averaged. The 1/12 term is added noise which results from converting back to a discrete value after averaging is performed. Further elaboration of the theoretical effect of image averaging is given in the thesis version of this work [30].

$$\sigma^2_{img\_th} = \frac{\sigma^2_{img}}{N_{\text{avgd}}} + \frac{1}{12}. \tag{17}$$

It may be useful in some cases to obtain an estimate of DIC uncertainty when using averaged images. To this end, Equations (16) and (17) can be combined to create Equation (18), which is the expected variance of a DIC displacement measurement due to image noise where each image used for DIC is the pixel-by-pixel mean of N_{avgd} consecutive images. Important to note is that σ^2_{img} here refers to the image noise present in the nonaveraged image, not the averaged image.

$$\sigma^2_{\text{DIC\_th}} \approx \frac{2\left((1/12) + \left(\sigma^2_{img}/N_{\text{avgd}}\right)\right)}{\text{SS}^2(\text{MIG})^2}. \tag{18}$$

3. Methods

The sample and equipment used for this work are similar to that used by Thai et al. in [6], as follows. A graphite rod purchased from http://GraphiteStore.com [32], which was milled in the center to have a square cross section of nominal width 7.62 mm (0.3 in), was lightly sanded and then speckled with Aremco Pyro-Paint 634-AL using a toothbrush speckling method [6]. The toothbrush method consists of dipping a toothbrush in paint and flicking the bristles toward the specimen such that paint lands on the

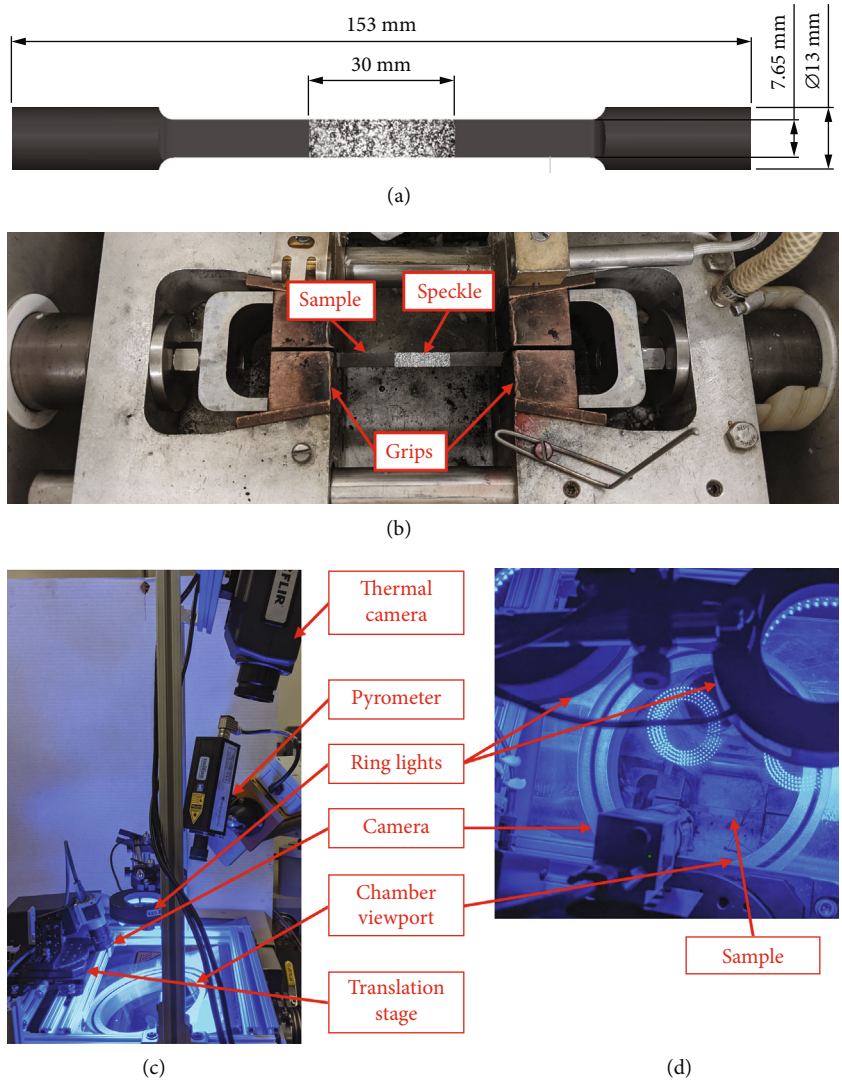

Figure 1: Experimental setup: (a) graphite sample dimensions, (b) sample mounted in the Gleeble, (c) photograph of the camera and lighting setup as viewed to one side of the load frame, and (d) additional photograph showing an overhead view of the camera and lighting setup looking into the viewing window.

specimen in a random pattern. The paint was dried for 2 hours at room temperature and then cured for 2 hours at 200°F per the manufacturer's instructions. The graphite sample and dimensions, as measured by digital calipers, are shown in Figure 1(a).

After the paint was fully cured, the sample was mounted in the vacuum test chamber of a Gleeble 1500D thermo-mechanical load frame. For this work, the loading mechanism for the load frame was disabled, and only the thermal component was used. Custom-made copper grips were used to mount the sample to the load frame. Heating the sample in the Gleeble was done by passing electrical current through the sample with temperature feedback using a type-k thermocouple, in this case Omega Alumel/Chromel wire welded at the junction. To ensure sufficient electrical conductivity between the grips and the sample, graphite powder was applied to the inside of the grips between the grip and the sample. The thermocouple was held against the sample using tension. Figure 1(b) shows the mounted sample.

Temperature measurement and control were accomplished using both a pyrometer aimed at the center of the sample and a type-k thermocouple offset 30 mm from the center. These measurements were initially calibrated against the temperature at the center of the sample as measured by a type-k thermocouple. The calibration method is described in detail in the thesis version of this work [30], which was based on the method used by Thai et al. in [6]. Details of the temperature calibration are omitted here for conciseness and because the accuracy of temperature measurement makes minimal impact on the conclusions in this work.

After the sample was mounted, the vacuum chamber of the Gleeble was sealed, and an aluminum frame with the camera equipment was mounted on top of the chamber. Camera equipment used included a micrometer-driven

Table 1: Test matrix for the room temperature studies. An asterisk (∗) indicates the baseline settings used to produce figures unless otherwise indicated.

Variable (units)	# of values	Values
Exposure time (μs)	13	210, 735, 1260, 1785, 2310, 2835, 3360, 3885, 4410*, 4935, 6125, 9065, 12005
Bit depth (bits)	2	8-bit*, 12-bit
N_{avgd} (images)	10	1*, 2, 3, 4, 8, 16, 32, 64, 128, 256
		×30 repeats

translation stage holding a single Basler Ace acA4600-10uc color camera and a pair of CCS LDR2-90BL2 blue LED ring lights. The Basler camera was equipped with an 8 mm lens set at aperture f/8. A Process Sensors Corporation Metis MQ11 2-color pyrometer was mounted to a separate fixture on the Gleeble. This fixture allowed the pyrometer to be moved out of the way when not in use without disturbing the optical equipment. The frame, camera, lights, and pyrometer are shown in Figures 1(c) and 1(d).

After mounting the camera, the vacuum chamber was evacuated to a pressure on the order of 10^{-2} torr to reduce oxidation of the sample at high temperatures.

3.1. Preliminary Noise Study. To determine the effect of bit depth on DIC uncertainty, it was necessary to ensure that a change in bit depth was not overshadowed by a high level of noise in the image. To this end, noise was varied by using a relatively noisy camera which had very small pixels, and then, image averaging was used to vary the apparent noise in the resulting images.

A series of 256 images was taken at room temperature for each combination of exposure time and bit depth in Table 1. Of these 256 images, N_{avgd} were randomly selected and averaged, and the averaged image was saved. This averaging process was repeated to produce 1 image for each of the 10 values of N_{avgd} shown. The process of image capture and averaging was then repeated 30 times, resulting in 30 images for each combination of settings in the table, which allowed for noise calculations to be performed based on the mean and standard deviation in each pixel. Baseline settings, indicated in the table using an asterisk (∗), were selected as a basis for comparison. In total, 199,680 raw images were collected to produce 7,800 averaged images of varying exposure time, bit depth, and N_{avgd}.

To quantify the properties of the camera used, several DIC-relevant metrics were calculated across each series of 256 single images and across each series of 30 averaged images. Because the camera is a color camera and the blue channel is of the most interest for high-temperature measurements, all metrics were calculated for only the blue channel. The following metrics were calculated:

(i) Z_1, Z_2, and Δ (see Equation (1))

(ii) MIG for the $N_{avgd} = 256$ image (see Equation (2)). The averaged image was used at the suggestion of Reu [33] in order to eliminate false gradients due to image noise. Derivatives were calculated using a central difference approximation

(iii) Image noise (σ^2_{img}) (see Equation (6))

(iv) B_{eff} (see Equation (12))

(v) σ_{img_th} (see Equation (17))

Once the images were collected and the noise and other metrics were calculated, DIC was performed, and the effects of bit depth and image averaging were analyzed. For DIC, the images were processed in VIC-2D using a 566×136 pixel region of interest (ROI), the ZNSSD criterion, a subset size of 27 pixels, and a subset spacing of 5 pixels. The mean and standard error of the DIC displacement measurement were then calculated for each image, similar to the method used in [34]. Important to note here is that these metrics are a measure of spatial statistics, meaning they are measured across some region in space, as opposed to temporal statistics which are measured at the same location across time (see [35] for a more in-depth discussion of spatial vs. temporal measurements). Although the two are not strictly the same, they are assumed equivalent for comparison purposes for the settings under investigation here since neither displacement nor strain is applied to the sample.

3.2. Room Temperature Exposure Time Study. After the effect of image averaging was validated, the effect of exposure time was explored for the room temperature data taken in the noise study (see Table 1). Because image averaging is used in this work to control the apparent noise in an image, the terms "high-noise" and "low-noise" are used when comparing nonaveraged ($N_{avgd} = 1$) and averaged ($N_{avgd} = 64$) images, respectively.

3.3. High-Temperature DIC Study. After taking and analyzing images at room temperature, the study was repeated at elevated temperature. For the high-temperature study, images were taken at varying exposure times, bit depths, temperatures, and values of N_{avgd} according to Table 2. Because the camera was not capable of taking a 4-bit image, an artificial 4-bit image set (denoted using "4d" meaning "4-derived") was created using the 8-bit images. Each 4d-bit image was created by taking an 8-bit image, dividing by a value of $2^4 = 16$, and saving the result as an integer-valued image. Image metrics and DIC were performed using the same methods and settings as in the room temperature study.

All correlations were performed with the reference image and displaced image obtained at the same temperature and position, such that results only show DIC error in

Table 2: Test matrix for the high-temperature study. An asterisk (∗) indicates the baseline settings used to produce figures unless otherwise indicated. Baseline settings are the same as for the room temperature studies.

Variable (units)	# of values	Values
Exposure time (μs)	13	210, 735, 1260, 1785, 2310, 2835, 3360,3885, 4410*, 4935, 6125, 9065, 12005
Bit depth (bits)	3	4d-bit, 8-bit*, 12-bit
N_{avgd} (images)	2	1*, 64
Temperature (°C)	11	25*, 500, 700, 900, 1000, 1100, 1200, 1300, 1400, 1500, 1600
		×2 repeats

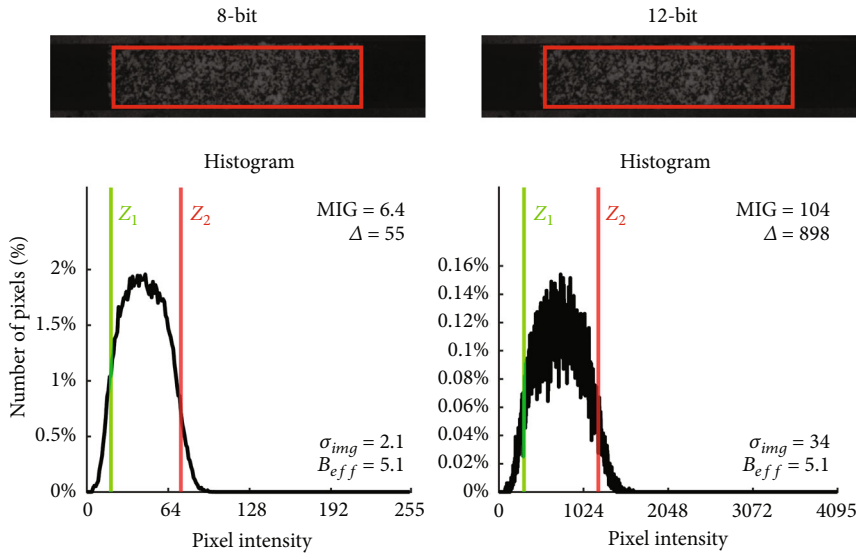

Figure 2: Example 8-bit and 12-bit images, where all other settings are baseline (baseline settings for this work are 8-bit, room temperature, nonaveraged images with a 4410 μs exposure time). Increasing bit depth scales the value of individual pixels to create the same image. Image noise also scales, but B_{eff} does not.

displacement, not thermal expansion or rigid body motion. After image acquisition and DIC were completed, image metrics and the mean and standard error of displacement were calculated across each image, and the results were analyzed.

4. Results

The following sections include results from the noise, exposure time, and high-temperature DIC studies.

4.1. Preliminary Noise Study. Sample images are shown in Figure 2, with accompanying histograms of the pixel distributions for each image. The images were obtained with the following baseline settings unless otherwise noted: room temperature, 8-bit, and nonaveraged images (N_{avgd} = 1, also referred to as high-noise images) with an exposure time of 4410 μs. These settings were chosen to most closely mimic standard test conditions and to minimize Δ while maintaining a minimum of 50 counts as suggested by Thai et al. for high-temperature DIC [6]. The figure includes both a baseline 8-bit image alongside the equivalent 12-bit image. Also included in the figure are the region of interest (ROI) used for calculations, the accompanying histogram, Z_1 (5th percentile marker), Z_2 (95th percentile marker), Δ (Equation (1)), MIG (Equation (2)), σ_{img} (Equation (6)), and B_{eff} (Equation (12)). Note also that since the calculation of statistical quantities requires multiple measurements, σ_{img} and B_{eff} were calculated across the series of 256 images, not from a single image like the other metrics were. In the figure, the histograms are of a roughly bell-curved shape with $\Delta > 50$, which suggests a good-quality speckle pattern with sufficient contrast for DIC measurements.

Comparing the 8- and 12-bit images in Figure 2 yields a few important observations. Visually, the two images look the same. The histograms have a similar shape except that the 12-bit histogram is thicker due to the larger variation of bin height from value to value. The primary difference between the two is the horizontal and vertical axes of the 12-bit histogram are roughly 16x smaller and larger, respectively, than that of the 8-bit image. This is expected since at 12-bit the camera uses a maximum integer value of $2^{12} - 1 = 4095$ to store intensities, and at 8-bit the camera only has a maximum integer value of $2^8 - 1 = 255$. Thus, the scales of both are expected to differ by a factor of $4095/255 \approx 16$.

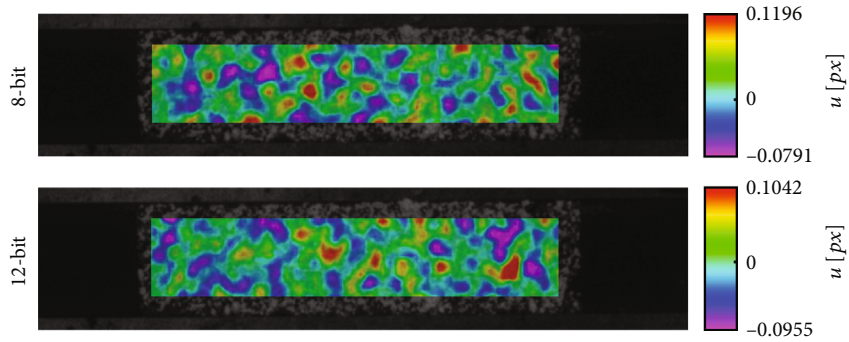

FIGURE 3: Measured horizontal displacement (u) of example 8-bit and 12-bit images. Displacement contours show approximately random behavior. Magnitudes of displacement (nominally zero) are of a similar range for both bit depths.

Example correlations of 8- and 12-bit images at otherwise baseline settings are shown in Figure 3. In the figure, the plots of horizontal displacement (u) exhibit a noisy, nonregular pattern having a similar range for both 8- and 12-bit nonaveraged images.

The effect of image averaging is shown in Figure 4, where σ_{img} and B_{eff} are plotted as a function of the number of images averaged for 8- and 12-bit images. Predicted values according to Equation (17) are also shown. Observed noise in the 8-bit images matches predicted values closely. For the 12-bit images, observed values deviate increasingly from expected values as the number of images increases and σ_{img} decreases. This deviation is likely due to nonrandom behavior in the images, such as periodic variation in light source intensity or vibration of the Gleeble. 12-bit averaged images show lower levels of noise and higher B_{eff} than their 8-bit counterparts when N_{avgd} is high. When $N_{\text{avgd}} > 64$, $B_{\text{eff}} > 8$ for 12-bit images taken with this camera and these settings (4410 μs, sample at room temperature).

DIC metrics were also evaluated as part of the noise study. In Figure 5(a), the $1 \cdot \sigma$ standard error of horizontal displacement is shown as a function of N_{avgd} for 8- and 12-bit images. For both bit depths, increasing the number of images averaged reduces DIC random error. In this portion of the figure, the 8- and 12-bit standard errors are nearly indistinguishable. However, it is not the absolute reduction of error which is of interest—it is the relative improvement which happens when moving from 8-bit to 12-bit images. To highlight this improvement, Figure 5(b) shows $\sigma_{u_{12}}/\sigma_{u_8}$, or the 12-bit standard error divided by the 8-bit standard error. The plot also includes a line of "no improvement" at $\sigma_{u_{12}}/\sigma_{u_8} = 1$, which represents no difference between the 8- and 12-bit measurements. The further $\sigma_{u_{12}}/\sigma_{u_8}$ is below this line, the more that using 12-bit images instead of 8-bit images improves the measurement. As N_{avgd} increases, which decreases image noise, moving from 8-bit to 12-bit images increasingly reduces DIC displacement standard error.

The reduction of DIC displacement standard error due to increasing bit depth becomes more pronounced at low exposure times. To show this effect, Figure 6 plots the same data as Figure 5(b) but adds in multiple exposure times. For

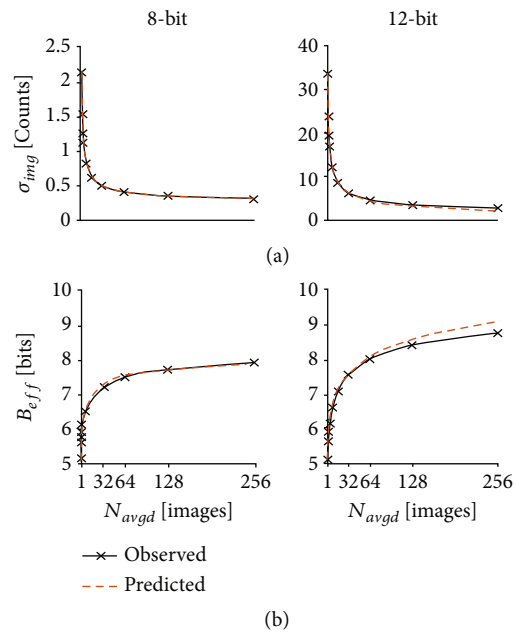

FIGURE 4: Observed and predicted image noise (a) and B_{eff} (b) as a function of the number of images averaged (N_{avgd}). Image noise tends to decrease as predicted by Equation (17) with some deviation, especially at lower noise/higher B_{eff}. Relative noise levels for 12-bit averaged images are lower than for 8-bit averaged images.

the 4410 μs exposure time images, moving from 8-bit to 12-bit images produced a 34% reduction in random error for $N_{\text{avgd}} = 256$. At a 735 μs exposure time, this reduction increased to 64%. Thus, at short exposure times for which images are relatively dark and small noise fluctuations can be relatively large in proportion to the true image, using more than 8 bits for image capture has a more pronounced benefit.

4.2. Room Temperature Exposure Time Study. The relationship between exposure time, image intensity, and image noise is shown for 8-bit images in Figure 7. Figure 7(a) shows the three sample images with the associated histograms plotted in the same format as Figure 2. Beneath the example images is a plot of Z_1, Z_2, Δ, and MIG vs. exposure

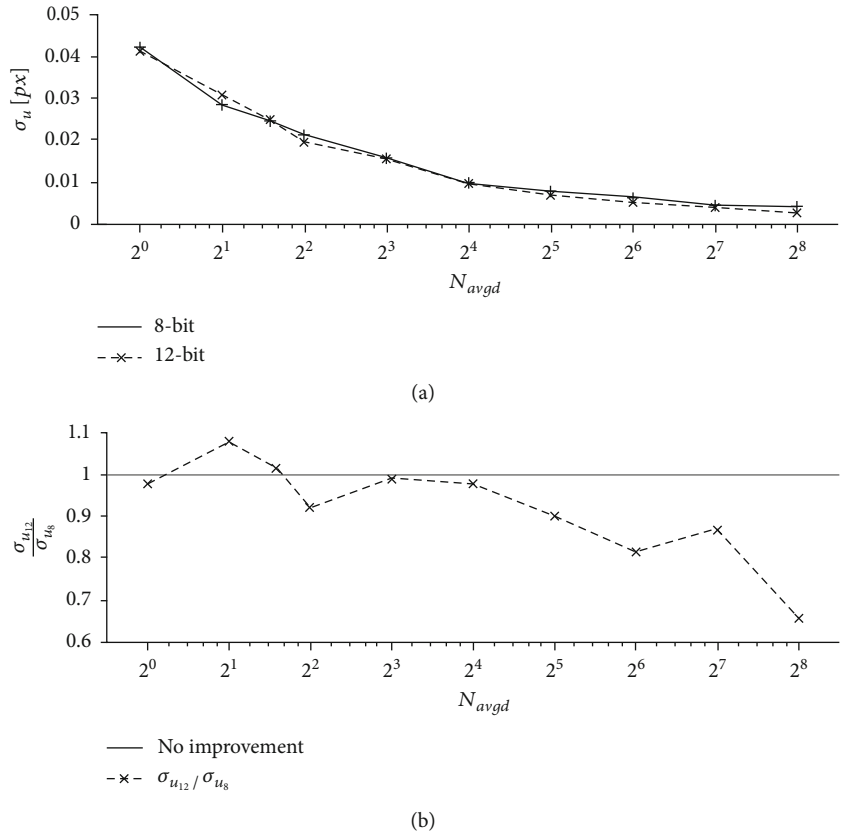

Figure 5: Comparison of 8- and 12-bit DIC displacement standard error as a function of N_{avgd} at otherwise baseline settings. (a) A plot of DIC displacement standard error vs. N_{avgd} for 8- and 12-bit images. (b) The 12-bit standard error divided by the 8-bit standard error (σ_{u12}/σ_{u8}), which illustrates the reduction in standard error achieved by using 12-bit images instead of 8-bit images for varying values of N_{avgd}. As N_{avgd} increases (noise decreases), the relative difference between 8- and 12-bit DIC random error increases.

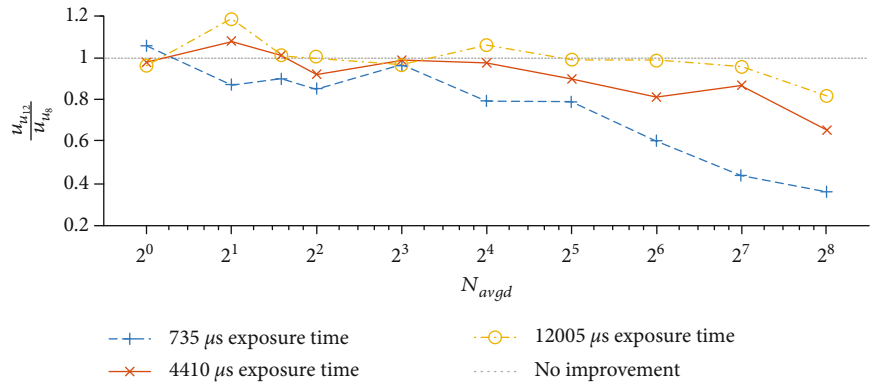

Figure 6: 12-bit DIC displacement standard error normalized by 8-bit standard error (σ_{u12}/σ_{u8}) for images at selected exposure times. Increasing bit depth has a larger effect on DIC displacement standard error at lower exposure times.

time. Figure 7(b) shows the two plots of σ_{img} and B_{eff} vs. exposure time, one for high-noise images ($N_{\text{avgd}} = 1$) and one for low-noise images ($N_{\text{avgd}} = 64$). All other settings are baseline. Based on the data shown, image intensity (Z_1 and Z_2) and contrast (Δ and MIG) have a linearly proportional relationship with exposure time. As for image noise, σ_{img} tends to increase with exposure time for both high-noise and low-noise images, which causes B_{eff} to decrease. Contrasting high-noise and low-noise images shows that the low-noise (averaged) images have much lower numerical values of noise and higher values of B_{eff}.

Figure 8 shows the same data as Figure 7 but for 12-bit images. As before, the histograms are "thicker," and pixel intensities are scaled in magnitude compared to the 8-bit images. The magnitude of B_{eff}, however, does not significantly increase for 12-bit high-noise images relative to the

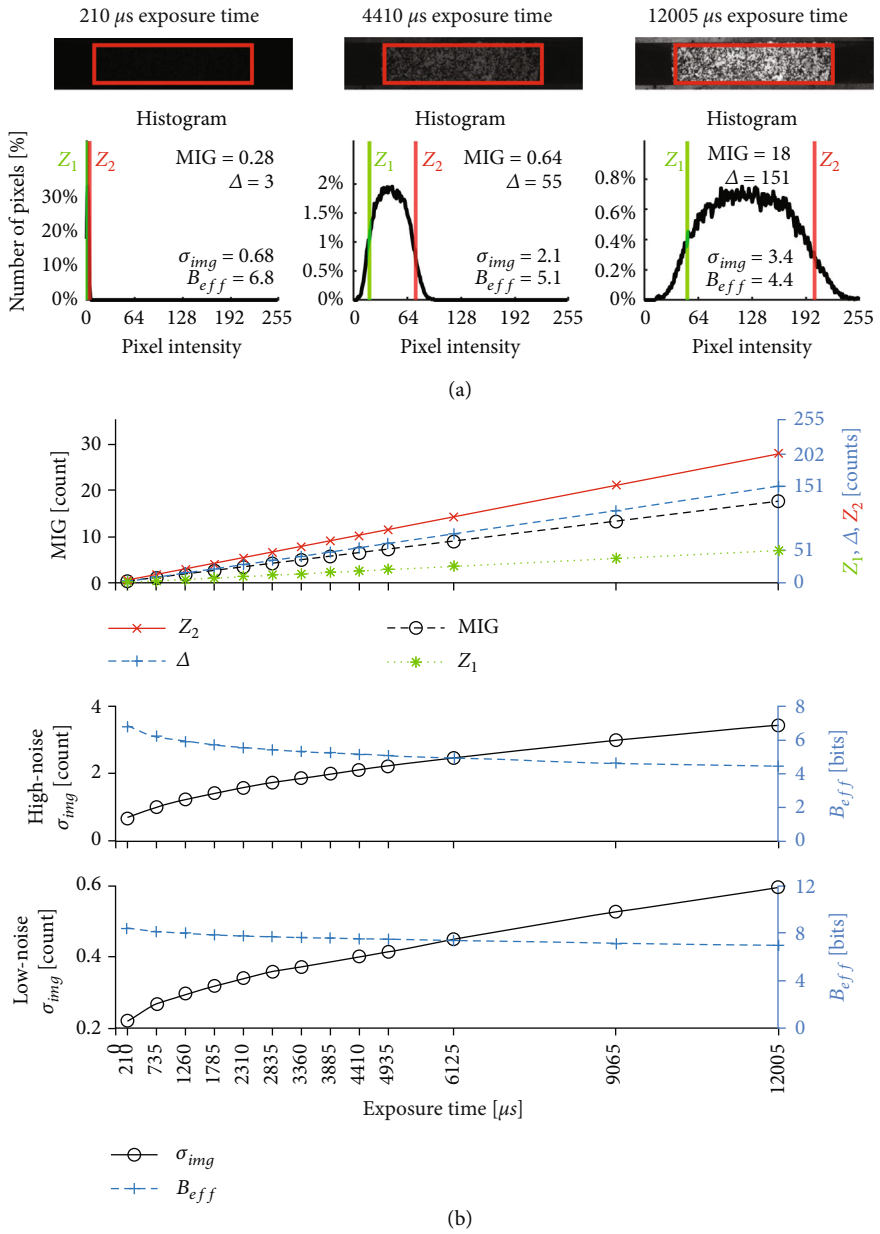

FIGURE 7: The relationship between image intensity, Z_2, Δ, MIG, Z_1, B_{eff}, and σ_{img} vs. exposure time. (a) Three example images with the associated histograms; (b) plots of each metric vs. exposure time. Maximum intensity, Δ, MIG, and minimum intensity each vary proportionally with exposure time. σ_{img} increases, and B_{eff} decreases as exposure time increases. Low-noise (averaged) images show lower noise and higher B_{eff} than their high-noise counterparts.

8-bit high-noise images. This suggests the increase in bit depth for high-noise (nonaveraged) images resulted in a negligible difference. Comparing B_{eff} for the low-noise images, however, shows that B_{eff} did increase for the 12-bit images relative to their 8-bit counterparts, especially at lower exposure times.

Unlike Figures 7 and 8, which show metrics of noise in noncorrelated images, Figure 9 shows DIC measurement uncertainty. Specifically, the figure shows as a function of exposure time: (i) the observed spatial standard error of horizontal displacement, (ii) the predicted temporal standard error from Vic-2D (where each data point shown is the square root of the mean of the squares of predicted uncertainty across all subsets in the image), and (iii) the predicted temporal standard error from Equation (15). All settings except exposure time and bit depth are baseline. The measured standard errors at the 210 μs exposure time, which were excluded from the plot window to make the plot easier to read, were 1.3 pixels and 0.53 pixels for 8- and 12-bit, respectively. Spatial standard error tends to be larger than predicted temporal standard error but follows the same trends with respect to exposure time. As exposure time increases, both observed and predicted standard error decrease asymptotically.

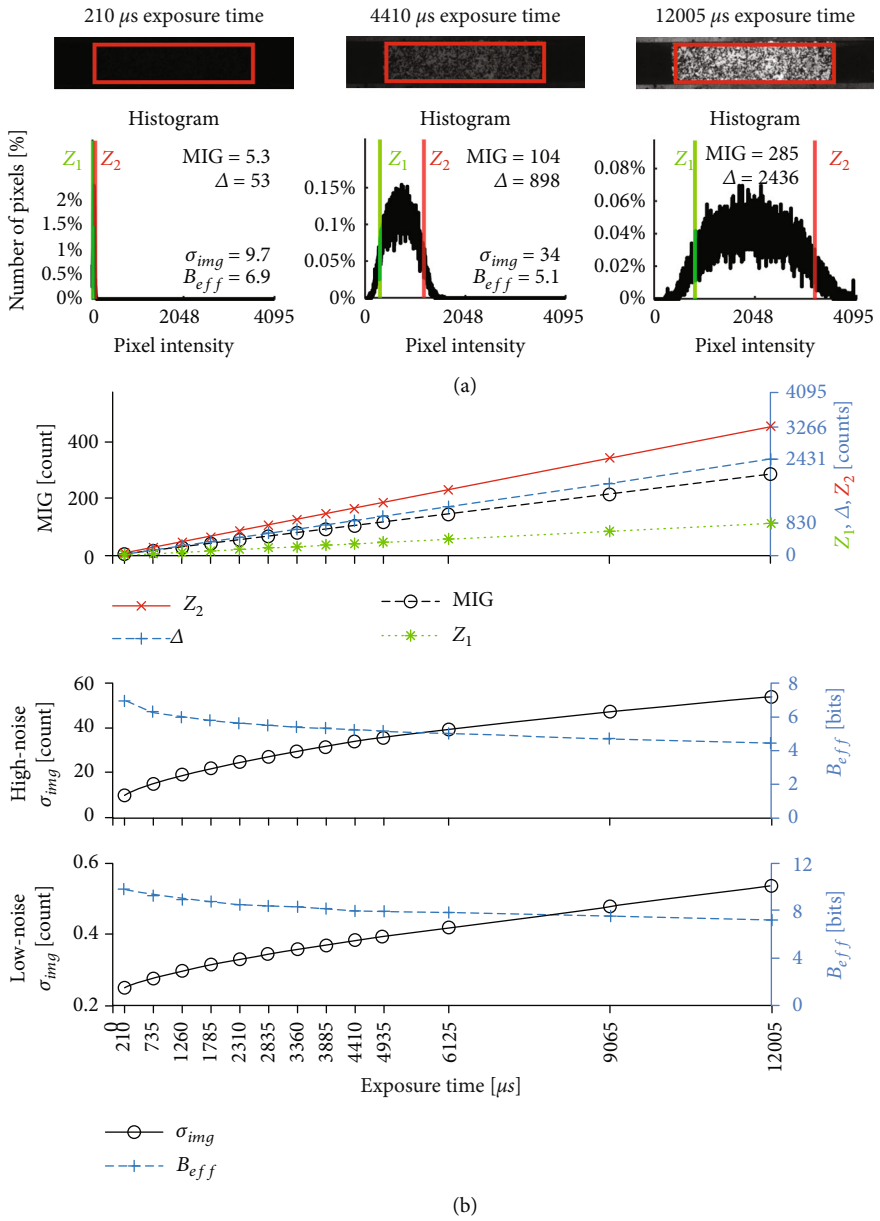

FIGURE 8: The relationship between image intensity, Z_2, Δ, MIG, Z_1, B_{eff}, and σ_{img} vs. exposure time for 12-bit images at otherwise baseline settings. (a) Three example images with the associated histograms; (b) plots of each metric vs. exposure time. Values and plots for 12-bit images hold the same trends as for 8-bit images (see Figure 7), but values are scaled in magnitude; the exception to this trend is B_{eff}, which is unchanged in the high-noise images and is only moderately larger in the low-noise images.

4.3. High-Temperature DIC Study. As was observed in [6], heating the specimen tends to increase the overall brightness of the image. Figure 10 shows a series of sample images with the associated histograms (Figure 10(a)) and a few image metrics as a function of temperature (Figure 10(b)) for the images taken under otherwise baseline settings. As temperature increased past ~900°C, the images increased in both brightness (Z_2) and contrast (Δ and MIG) until the images began to saturate at ~1400°C. After this point, the images continued to brighten, but contrast decreased until both Δ and MIG fell to zero.

Speckle pattern inversion was also observed, in which dark pixels switch to light pixels and vice versa as temperature increases [22, 23, 36]. The inversion can be seen by comparing the 25°C image to the 1300°C image in Figure 10. Speckle pattern inversion can make DIC difficult or impossible because subsets in the high-temperature image display the opposite of what they were in the room temperature image. Because images in this work were correlated using reference images and displaced images at the same temperature, the inversion was not prohibitive for DIC, but reduced contrast at the point of inversion did cause unique correlation behavior as discussed later in Figures 11 and 12.

Although Figure 10 shows brightness and contrast trends which are somewhat characteristic of all high-temperature images taken, they are limited to a single

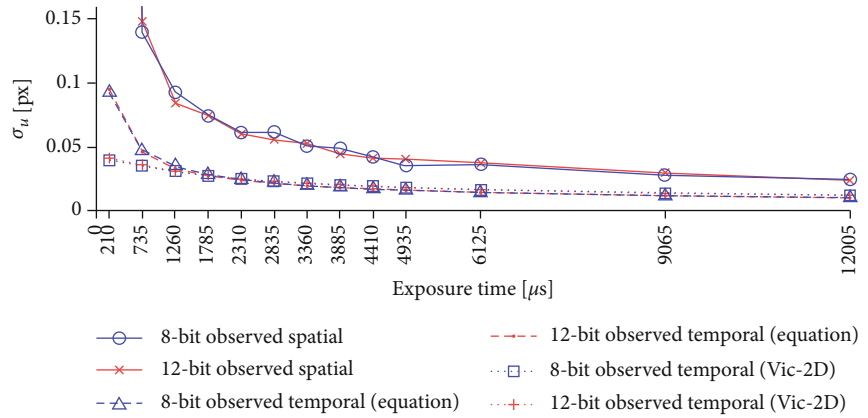

FIGURE 9: 8- and 12-bit observed and predicted displacement standard error as a function of exposure time where all other settings are baseline. Predicted values are calculated using either Equation (15) or reported values from Vic-2D. Both predicted and observed DIC displacement standard error decrease asymptotically as exposure time increases.

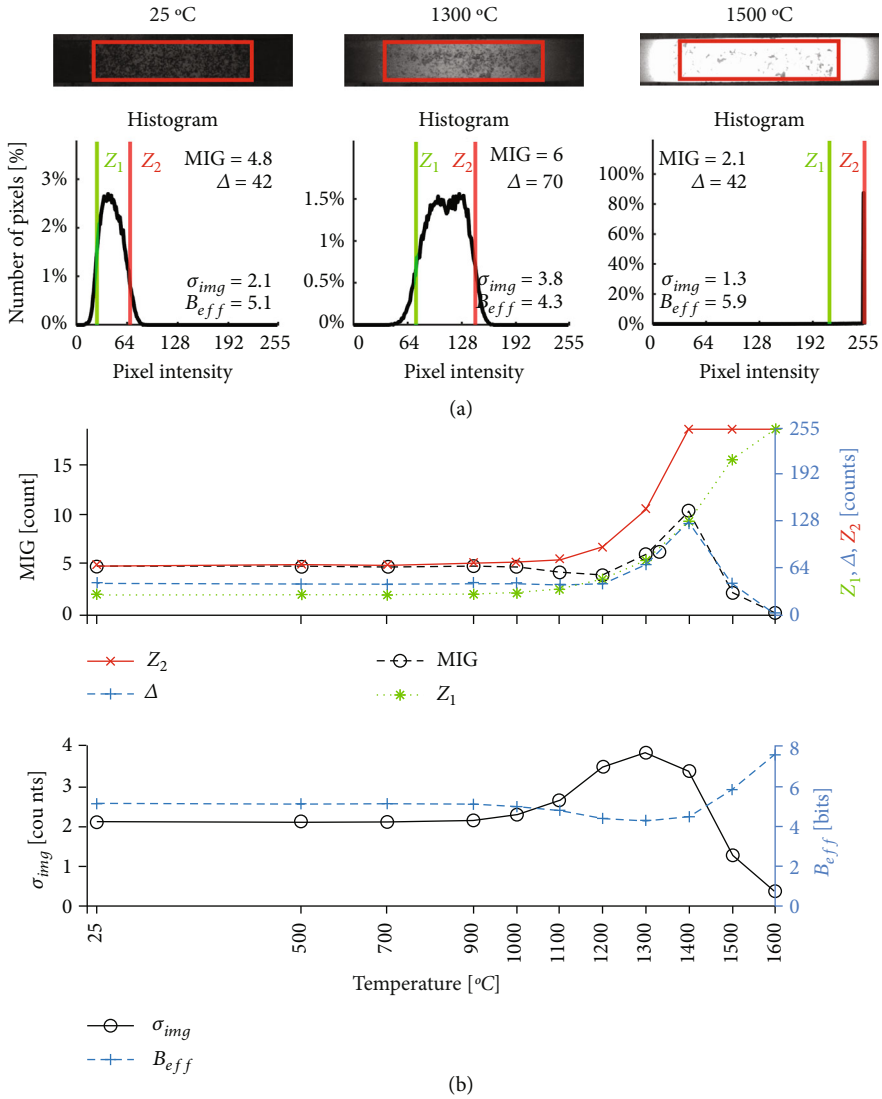

FIGURE 10: The relationship between image intensity, Z_2, Δ, MIG, Z_1, B_{eff}, and σ_{img} vs. temperature. (a) Three example images with the associated histograms; (b) plots of each metric vs. temperature. Prior to saturation, increases in temperature tend to increase both brightness and contrast, but after saturation begins, increases in temperature reduce contrast.

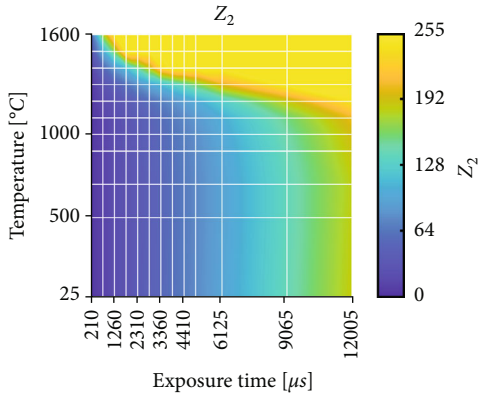

FIGURE 11: Δ and MIG for all exposure times, bit depths, and temperatures in the high-temperature study. Δ and MIG both follow nearly the same trends with respect to exposure time, temperature, and bit depth.

exposure time. Figures 11 and 13 expand upon this, first showing Z_2 for 8-bit low-noise images in Figure 13 and then showing Δ and MIG for multiple bit depths in Figure 11.

In Figure 13, Z_2 is shown as a function of exposure time and temperature. White gridlines denote an actual temperature or exposure time used, and the intersection of each gridline is the location of a measured data point. All other regions in the colormap are linearly interpolated values. At room temperature, increasing exposure time increases Z_2. As temperature increases, Z_2 remains constant until some temperature above roughly 900°C depending on the exposure time; after this point, Z_2 then increases until saturation occurs. The yellow region in the top right of the figure represents images with varying levels of saturation—a region that should be avoided for DIC measurements.

In Figure 11, multiple plots of Δ and MIG are presented in the same format as Figure 13 and are organized by bit depth. The plots all show color contours which are similar to one another. At room temperature, both Δ and MIG increase with exposure time. As temperature increases through the onset of saturation (the lower boundary of the yellow region in Figure 13), Δ and MIG peak and then diminish. The peaks in Δ and MIG occur at approximately the same location as the lower boundary of the saturated region in Figure 13. At lower exposure times, image saturation and peak Δ and MIG occur at higher temperatures. In the region of 1200-1300°C, the peak values of Δ and MIG are lower than at other temperatures; this is likely because the image is only partway through the process of speckle pattern inversion, which would reduce contrast.

Comparing the plots of Δ and MIG with respect to each other and with respect to bit depth is also informative. Δ and MIG follow roughly the same trends as each other with respect to exposure time and temperature, though there is some difference between the two around the point of speckle inversion (1200-1300°C). As bit depth increases, plot scale increases but the contours do not change significantly for either Δ or MIG.

Figure 12 shows the standard error of horizontal displacement as a function of exposure time and temperature for all bit depths in Table 2. The figure includes several plots in the same format as Figure 13 organized by bit depth and by high-noise (N_{avgd}=1) vs. low-noise (N_{avgd} = 64).

A few observations are important here which are true for all of the plots in Figure 12. As observed previously, at room temperature, DIC standard error decreases as exposure time increases. As temperature increases past 1100°C, however, the region where random error is lowest shifts toward lower exposure times. This low point in σ_u occurs at roughly the same location as the MIG and Δ peaks observed in in Figure 11. Increasing temperature or exposure time beyond this point leads to image saturation, an increase in standard error, and eventual failure of the correlation as shown by the blank regions in the upper right corner of the plots.

Comparing between bit depths in Figure 12 yields a few key observations. Moving from 4-bit to 8-bit images produces a dramatic decrease in random error for both high-noise and low-noise images. For high-noise images, the remaining plots (8-bit and 12-bit) are nearly identical—no improvement resulted from increasing bit depth. For low-noise images, however, moving from 8-bit to 12-bit did reduce DIC random error at the same exposure times and temperatures. This is seen at lower temperatures as a shift of the blue and violet region to the left of the plot as bit depth increases. The difference in behavior between high-noise and low-noise images is as expected, since increasing bit depth is only expected to reduce DIC error if image noise is sufficiently low (see Equation (16)).

5. Discussion

The first two subsections below discuss the effect of changing bit depth on DIC displacement uncertainty in the room temperature and high-temperature studies. The remaining section is a discussion of the Δ metric for bit depths other than 8-bit.

5.1. Room Temperature Studies. High image noise is a key factor for whether increasing bit depth will improve DIC. In the discussion of Equation (16), it was predicted that if image noise from sources other than quantization ($\sum\sigma_i^2$) is significantly higher than 1/12, then increasing bit depth is not expected to produce a significant difference in DIC displacement uncertainty. Inspection of Figures 3–6 shows that, for the camera used in this study, when images are not averaged, no significant difference exists between DIC displacement results using 8-bit vs. 12-bit images. Taking the baseline images as an example, σ_{img} for these images was 2.11 counts. Taking out quantization noise (using the equation $\sqrt{\sigma_{img}^2 - 1/12}$) results in a standard error of 2.09 counts—only 0.02 counts difference. Thus, it is not surprising that no significant difference was achieved by increasing bit depth under the baseline settings, since quantization noise was only a small portion of the total noise in the 8-bit images.

In contrast to the high-noise images, correlations of low-noise images were shown to benefit from higher bit depth under a range of settings. As was seen in Figure 6, the effect

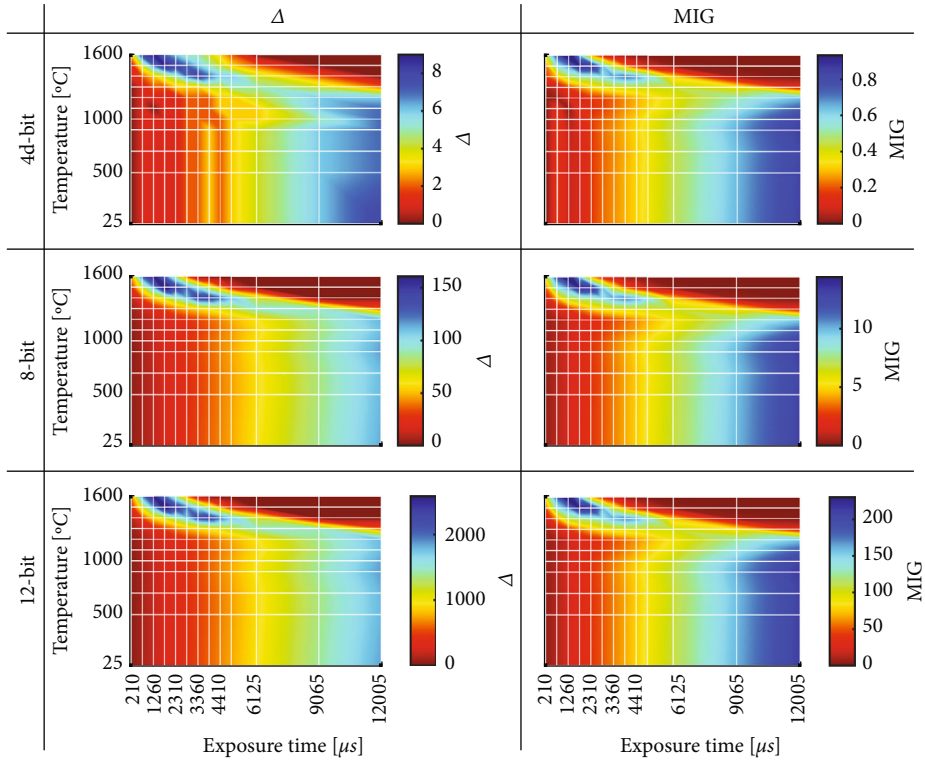

Figure 12: DIC spatial standard error for high-noise ($N_{avgd} = 1$) and low-noise ($N_{avgd} = 64$) images between 25 and 1600°C. If image noise is low enough, increasing bit depth reduces DIC standard error.

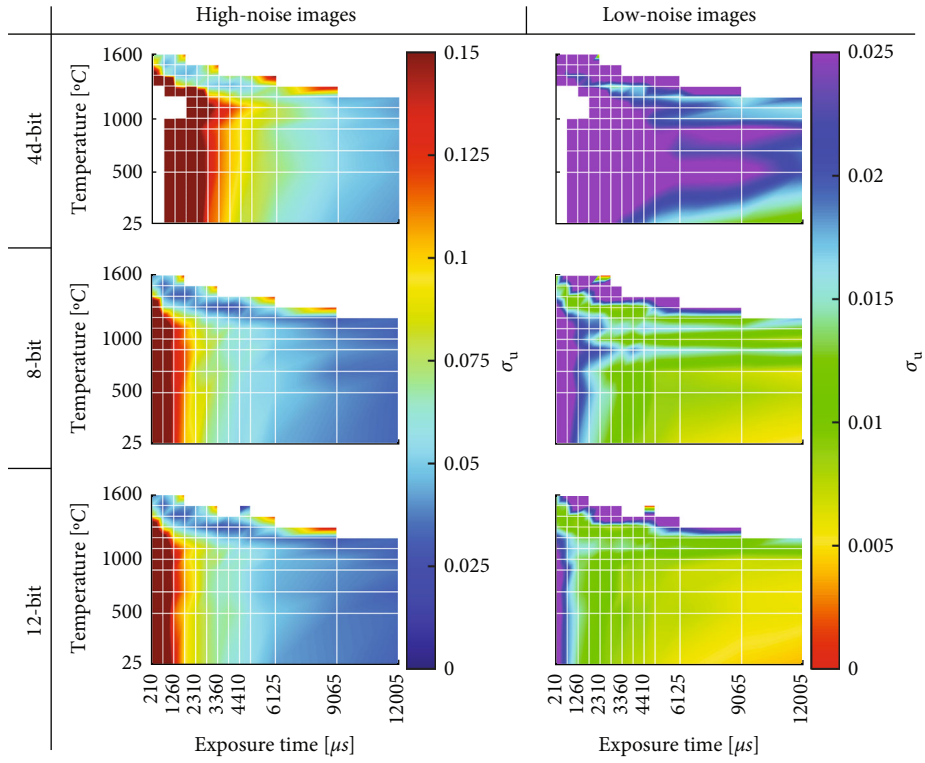

Figure 13: Z_2 of all 8-bit images vs. exposure time and temperature. MIG tends to increase with exposure time and temperature until saturation occurs, after which MIG quickly decreases.

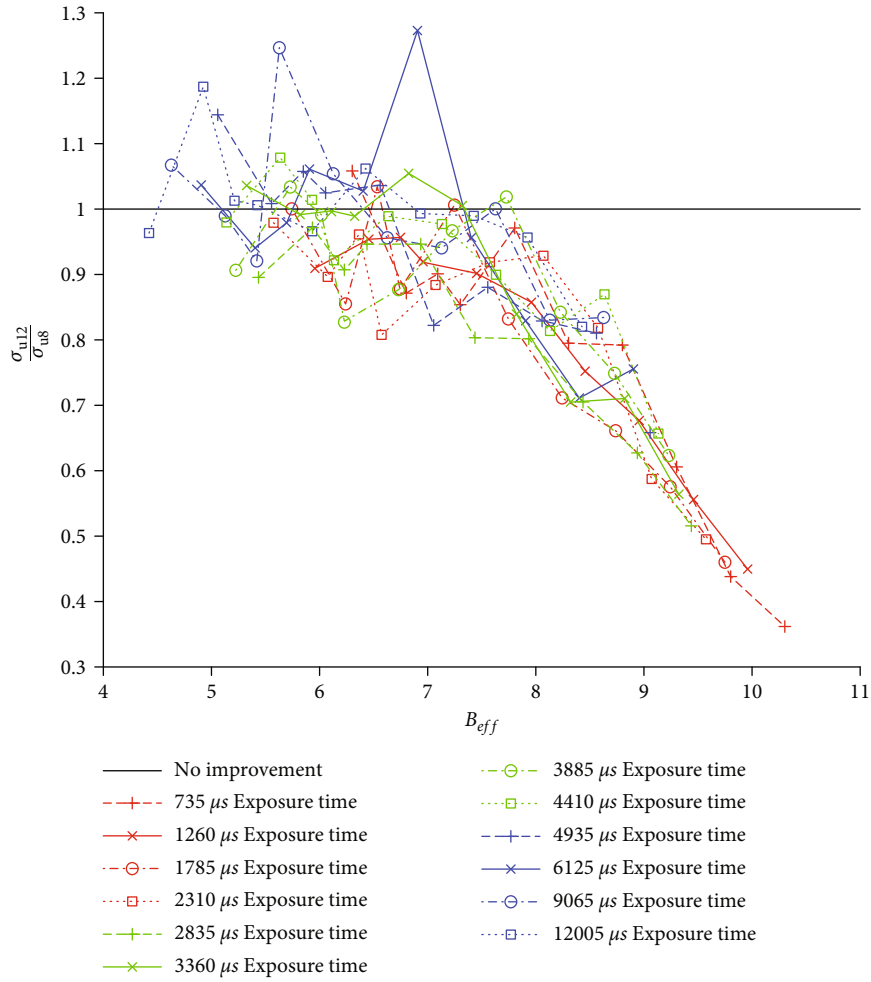

FIGURE 14: σ_{u12}/σ_{u8} vs. B_{eff} at room temperature for a wide range of settings. As B_{eff} increases, using 12-bit images instead of 8-bit images for DIC results in an increasing reduction in DIC random error.

on DIC random error due to increasing from 8- to 12-bit images shows significant improvement as N_{avgd} increases beyond a given threshold. However, when plotting with respect to N_{avgd}, this improvement begins at different thresholds for different exposure times. Because image averaging is used to control noise in this work, it is helpful to plot the data in Figures 5 and 6 as a function of B_{eff} (which is a measure of image noise) instead of N_{avgd}. This is shown in Figure 14. Here, similar to Figure 6, the 12-bit standard error is normalized by the 8-bit standard error ($\sigma_{u_{12}}/\sigma_{u_8}$, which indicates the amount of error in the 12-bit image relative to its 8-bit counterpart) and plotted as a function of B_{eff}. Recall that, as in Figure 5(b), if a data point is below the line of no improvement, moving from 8-bit to 12-bit images improves DIC. At lower values of B_{eff}, the data tend to hover around the line of no improvement. As B_{eff} increases, the data show a downward trend indicating reduced error at 12 bits. This downward trend begins as early as $B_{\text{eff}} = 6$. Once $B_{\text{eff}} \geq 8$, all data points show at least some improvement from using 12-bit images instead of 8-bit images.

Based on the data shown, one way to determine the appropriate number of bits for DIC images prior to the start of testing is to find B_{eff} for the experimental setup in question. This should be done by taking a series of at least 30 images at the maximum bit depth of the camera, calculating σ_{img} within the region of interest using Equation (6), and calculating B_{eff} using Equation (12). Because the downward trend in Figure 14 begins when B_{eff} is (roughly) between 6 and 7, it is recommended that the number of bits used to capture and store images be about 1-2 bits greater than B_{eff}. Increasing bit depth beyond this number may increase required storage space but is not likely to produce an improvement in DIC uncertainty. The ability to use B_{eff} to determine the appropriate number of bits for DIC images is significant because B_{eff} can be calculated prior to Digital Image Correlation, allowing the user to determine whether 8-bit or higher-bit images should be used before the experiment begins.

5.2. High-Temperature DIC Study. Increased bit depth can be leveraged to reduce exposure time without compromising measurement precision. Consider, for example, the plots of displacement standard error vs. exposure time for 8- and 12-bit low-noise room temperature images in Figure 15.

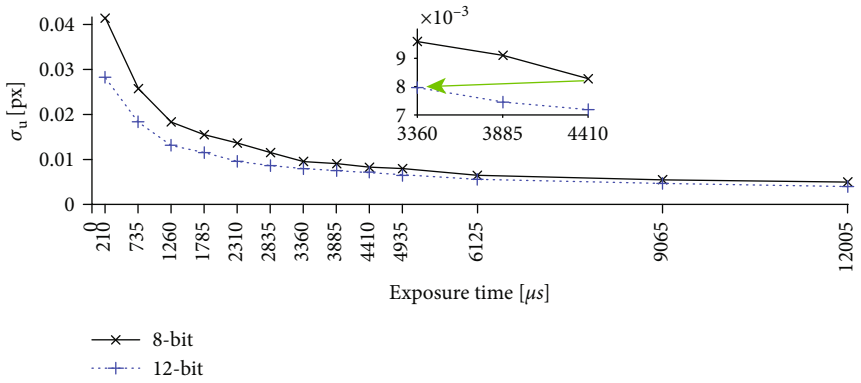

FIGURE 15: σ_u vs. exposure time for 8d-bit, 10d-bit, and 12-bit low-noise images (room temperature, $N_{\text{avgd}} = 64$). For low-noise images, 12-bit DIC data exhibit similar standard error values to 8-bit images but at lower exposure times. An enlarged section of the range from 3360 to 4410 μs is also shown with a green arrow representing the transition from 8-bit 4410 μs exposure time images (the baseline image set) to 12-bit 3360 μs exposure time images, which transition reduces both contrast and DIC random error.

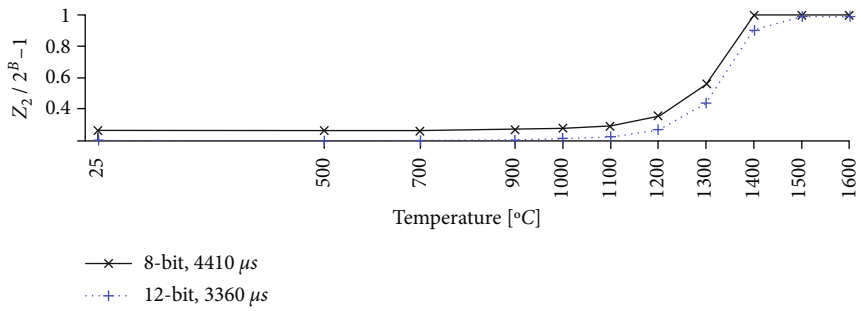

FIGURE 16: Z_2 vs. temperature under selected settings. All images are low-noise ($N_{\text{avgd}} = 64$). Images with a 3360 μs exposure time saturate at a higher temperature than images at a 4410 μs exposure time.

The standard error of the 8-bit, 4410 μs correlations (the baseline images), was 0.0083 px. On the 12-bit curve, the 3360 μs images had a standard error of 0.0080. This range of exposure times is shown as an enlarged section in the figure. By using 12-bit 3360 μs images instead of 8-bit 4410 μs images, indicated by the green arrow in the enlarged section, the brightness of the images can be reduced with no loss in measurement precision.

By reducing the exposure time, the maximum temperature range of DIC can be increased. As a continuation of the example in the previous paragraph, Figure 16 shows $Z_2/(2^B - 1)$, a normalized metric of near-maximum pixel intensity, for 12-bit 3360 μs and 8-bit 4410 μs low-noise images. As temperature increases, the maximum intensity of both image sets increases until saturation near 1400°C. Note, however, that the 4410 μs images saturate at (or before) 1400°C, whereas the 3360 μs images saturate sometime after 1400°C but before 1500°C. This means that increasing bit depth and reducing exposure time can allow for taking nonsaturated images at higher temperatures without a reduction in DIC precision. Although the difference in temperatures is small here, roughly on the order of 10°C based on the trajectory of the curves shown, a different experimental setup or method (e.g., a camera with lower noise or more images averaged) could increase this difference. If image noise is low enough, bit depth and exposure time can be leveraged to increase the maximum temperature range of DIC.

5.3. The Δ Metric at Varying Bit Depths. Comparison of the plots of σ_u in Figure 12 for varying bit depths shows that for high-noise images, increasing bit depth beyond 8 bits does not significantly change DIC random error. However, increasing bit depth does increase Δ (see Figure 11). Thus, Δ alone is not a good indicator for whether an image has sufficient contrast when using something other than the standard 8-bit images—a new recommendation is needed.

One method to convert Δ into a more general metric of image quality is to convert Δ into a percentage of the maximum value as shown in Equation (19). Converting Δ to a percentage is consistent with the discussion of contrast in the iDICs Good Practices Guide [25], which recommends a minimum contrast of around 20% for an 8-bit camera [25]. However, the guide does not give specific guidance for different bit depths.

$$\Delta_{\%} = \frac{\Delta}{\left(2^B - 1\right)} \times 100\%. \tag{19}$$

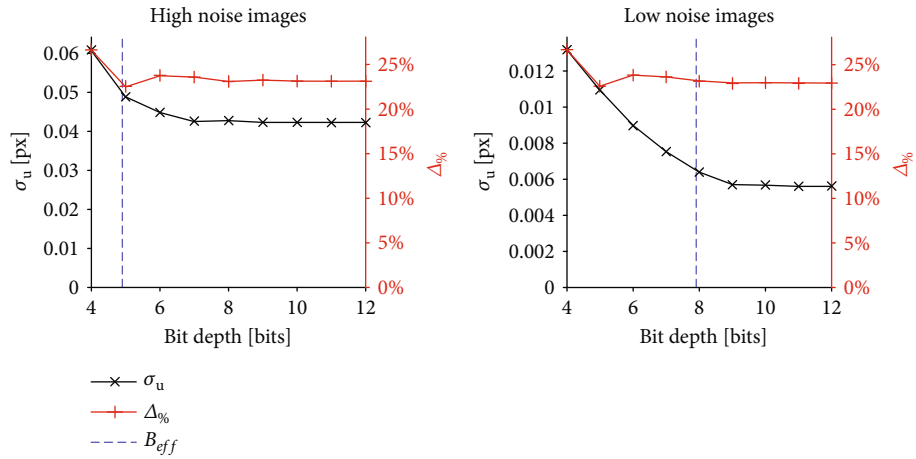

FIGURE 17: σ_u and $\Delta_{\%}$ vs. bit depth at otherwise baseline settings. For $B \geq 8$ bits, both σ_u and $\Delta_{\%}$ remain consistent as bit depth increases.

Figure 17 shows σ_u and $\Delta_{\%}$ vs. bit depth for room temperature, 6125 μs exposure time, high-noise (nonaveraged), and low-noise ($N_{\text{avgd}} = 64$) images. For these data, a new DIC dataset was created using images at varying bit depths; images for the new dataset were derived from the 12-bit room temperature images in the high-temperature study using the same conversion process that was used to produce the 4d-bit data in the high-temperature study. B_{eff} for the 12-bit image is also shown in both plots as a reference, where B_{eff} is calculated directly using σ^2_{img} for the high-noise images and using $\sigma^2_{img\_\text{exp}}$ (see Equation (17)) for the low-noise images.

In both plots in Figure 17, $\Delta_{\%}$ takes on similar values for both the high-noise and low-noise image sets. Observing how $\Delta_{\%}$ changes with bit depth shows that $\Delta_{\%}$ is generally constant but varies more at low bit depths than at higher bit depths; this variation at low bit depths is attributed to quantization effects (rounding). Also in both plots, σ_u tends to decrease with increasing bit depth until a certain point and then remains constant regardless of bit depth. This levelling-out point occurs roughly 1-2 bits higher than B_{eff}, which reinforces the earlier recommendation that the number of bits used for DIC images should be at least 1-2 bits greater than B_{eff} in order to minimize both DIC random error and image storage space. Looking specifically at $B \geq 8$ for high-noise images, both $\Delta_{\%}$ and σ_u stay nearly constant as bit depth increases. Thus, for a camera with relatively high noise, increasing bit depth will not significantly affect DIC random error. As such, it remains a good rule of thumb to ensure a minimum of 20% contrast between dark and light features for DIC images regardless of whether 8-bit or higher-bit images are used.

Important to note here is that the 20% recommendation is only a starting point; if possible, the DIC uncertainty/error should be assessed directly prior to the experiment. This allows the user to determine whether the DIC measurement is precise enough for the experimental work and/or whether contrast can be safely reduced while maintaining sufficient measurement precision. As a rule of thumb for required measurement precision, Reu recommends that σ_u should be less than 0.005 pixels [33]. Random error can be calculated by taking images of the sample with zero nominal displacement or strain, performing DIC, and calculating the standard deviation of subset displacement.

6. Conclusions

In summary, all images have some noise associated with them (σ_{img}) which can impact the uncertainty of DIC measurements (σ_u for displacement u). The noise depends on numerous factors which include but are not limited to the sensor format (e.g., pixel size), camera settings (e.g., gain and exposure time), and quantization error as a result of bit depth. In the case of high-temperature DIC, the noise also depends on light emitted due to blackbody radiation. It is well-understood that one can mitigate the emitted light by reducing exposure time while still maintaining sufficient contrast. We have shown that, if image noise is sufficiently low on a camera capable of variable bit depth, one can use that bit depth to afford modestly shorter exposure times and thereby extend DIC to higher temperatures. For the purposes of this study, noise was varied by using a relatively noisy camera which had very small pixels and then averaging together many images to reduce noise.

To assess whether a particular test setup can be improved by higher bit depth, we recommend the following simple procedure:

(1) Prior to deforming the sample, record a series of at least 30 static images using the highest bit depth available for that camera

(2) Find the standard error of the pixel intensity (σ_{img}) by first finding the standard deviation in each pixel across all images and then taking the square root of the sum of the squares of those standard deviations

(3) Use this value in Equation (12) to compute the effective number of bits, B_{eff}

(4) Choose the smallest bit depth greater than or equal to B_{eff} +2. Beyond this value, any improvements to DIC will be negligible, but images recorded with bit depths between 9 and 16 require twice as much memory as images with bit depths of 8 or lower

It should be noted that although this procedure was developed for high-temperature DIC experiments, it can be applied to reduce uncertainty in other low-noise DIC applications as well.

It should also be noted that, in our lab's previous high-temperature DIC papers, we recommended that for an 8-bit camera, one should set the exposure time as short as possible while maintaining a contrast of $\Delta > 50$ (see Equation (1)). When applied to other bit depths, this recommendation can be generalized to $\Delta_{\%} \geq 20\%$ of the dynamic range of the camera (see Equation (19)).

Data Availability

The data used to support the findings of this study are available from the corresponding author upon reasonable request.

Disclosure

Any opinions, findings, and conclusions or recommendations expressed by this publication are those of the authors and do not necessarily reflect the views of the U.S. Department of Energy or Nuclear Regulatory Commission.

Conflicts of Interest

The authors have no conflicts of interest to disclose as relate to this manuscript.

Acknowledgments

This material is based upon work supported by the U.S. Department of Energy's Nuclear Energy University Program (NEUP) Integrated Research Project (IRP) under agency award number DE-NE-0008531. WDC would also like to acknowledge support from a graduate fellowship from the U.S. Nuclear Regulatory Commission (NRC) under award number 31310019M0044.

References

[1] P. Reu, "Introduction to digital image correlation: best practices and applications," *Experimental Techniques*, vol. 36, no. 1, pp. 3-4, 2012.

[2] Y. L. Dong and B. Pan, "A review of speckle pattern fabrication and assessment for digital image correlation," *Experimental Mechanics*, vol. 57, no. 8, pp. 1161–1181, 2017.

[3] ""Planck's radiation law | Definition, formula, & facts," Encyclopedia Britannica," October 2020, https://www.britannica.com/science/Plancks-radiation-law.

[4] T. Q. Thai, R. J. Rowley, R. S. Hansen, and R. B. Berke, "How light emitted at high temperature affects common digital image correlation algorithms," *Measurement Science and Technology*, vol. 32, no. 12, article 129401, 2021.

[5] J. S. Lyons, J. Liu, and M. A. Sutton, "High-temperature deformation measurements using digital-image correlation," *Experimental Mechanics*, vol. 36, no. 1, pp. 64–70, 1996.

[6] T. Q. Thai, R. S. Hansen, A. J. Smith, J. Lambros, and R. B. Berke, "Importance of exposure time on DIC measurement uncertainty at extreme temperatures," *Experimental Techniques*, vol. 43, no. 3, pp. 261–271, 2019.

[7] B. M. B. Grant, H. J. Stone, P. J. Withers, and M. Preuss, "High-temperature strain field measurement using digital image correlation," *Journal of Strain Analysis for Engineering Design*, vol. 44, no. 4, pp. 263–271, 2009.

[8] M. D. Novak and F. W. Zok, "High-temperature materials testing with full-field strain measurement: experimental design and practice," *The Review of Scientific Instruments*, vol. 82, no. 11, article 115101, 2011.

[9] Z. Pan, S. Huang, Y. Su, M. Qiao, and Q. Zhang, "Strain field measurements over 3000 °C using 3D-digital image correlation," *Optics and Lasers in Engineering*, vol. 127, article 105942, 2020.

[10] X. Chen, N. Xu, L. Yang, and D. Xiang, "High temperature displacement and strain measurement using a monochromatic light illuminated stereo digital image correlation system," *Measurement Science and Technology*, vol. 23, no. 12, article 125603, 2012.

[11] B. Pan, D. Wu, and L. Yu, "Optimization of a three-dimensional digital image correlation system for deformation measurements in extreme environments," *Applied Optics*, vol. 51, no. 19, pp. 4409–4419, 2012.

[12] X. Guo, J. Liang, Z. Tang, B. Cao, and M. Yu, "High-temperature digital image correlation method for full-field deformation measurement captured with filters at 2600°C using spraying to form speckle patterns," *Optical Engineering*, vol. 53, no. 6, pp. 063101–063101, 2014.

[13] P. Meyer and A. M. Waas, "Measurement of in situ-full-field strain maps on ceramic matrix composites at elevated temperature using digital image correlation," *Experimental Mechanics*, vol. 55, no. 5, pp. 795–802, 2015.

[14] J. Blaber, B. S. Adair, and A. Antoniou, "A methodology for high resolution digital image correlation in high temperature experiments," *The Review of Scientific Instruments*, vol. 86, no. 3, article 035111, 2015.

[15] W. Wang, C. Xu, H. Jin, S. Meng, Y. Zhang, and W. Xie, "Measurement of high temperature full-field strain up to 2000 °C using digital image correlation," *Measurement Science and Technology*, vol. 28, no. 3, article 035007, 2017.

[16] T. Q. Thai, A. J. Smith, R. J. Rowley, P. R. Gradl, and R. B. Berke, "Change of exposure time mid-test in high temperature DIC measurement," *Measurement Science and Technology*, vol. 31, no. 7, article 075402, 2020.

[17] R. B. Berke and J. Lambros, "Ultraviolet digital image correlation (UV-DIC) for high temperature applications," *The Review of Scientific Instruments*, vol. 85, no. 4, article 045121, 2014.

[18] Y. Dong and B. Pan, "In-situ 3D shape and recession measurements of ablative materials in an arc- heated wind tunnel by UV stereo-digital image correlation," *Optics and Lasers in Engineering*, vol. 116, pp. 75–81, 2019.

[19] E. K. Nickerson and R. B. Berke, "Ultraviolet diffraction assisted image correlation (UV-DAIC) for single-camera 3D

strain measurement at extreme temperatures," *Experimental Mechanics*, vol. 58, no. 6, pp. 885–892, 2018.

[20] R. S. Hansen, T. J. Bird, R. Voie, K. Z. Burn, and R. B. Berke, "A high magnification UV lens for high temperature optical strain measurements," *The Review of Scientific Instruments*, vol. 90, no. 4, article 045117, 2019.

[21] E. M. C. Jones, E. C. Quintana, P. L. Reu, and J. L. Wagner, "X-Ray stereo digital image correlation," *Experimental Techniques*, vol. 44, no. 2, pp. 159–174, 2020.

[22] T. Thai, *Improvement of Ultraviolet Digital Image Correlation (UV-DIC) at Extreme Temperatures*, Grad. Theses Diss, 2020.

[23] T. Q. Thai, J. Ruesch, P. R. Gradl, T. T. Truscott, and R. B. Berke, *Speckle Pattern Inversion in High Temperature DIC Measurement*, Exp. Tech, 2022.

[24] P. Reu, "Stereo-rig design: lighting-part 5," *Experimental Techniques*, vol. 37, no. 3, pp. 1-2, 2013.

[25] I. Jones, *A Good Practices Guide for Digital Image Correlation*, 2018.

[26] B. Pan, Z. Lu, and H. Xie, "Mean intensity gradient: an effective global parameter for quality assessment of the speckle patterns used in digital image correlation," *Optics and Lasers in Engineering*, vol. 48, no. 4, pp. 469–477, 2010.

[27] J. H. Reed, *Software Radio : A Modern Approach to Radio Engineering*, Prentice Hall, Upper Saddle River, N.J, 2002.

[28] D. D. Wackerly, W. Mendenhall, and R. L. Scheaffer, *Mathematical Statistics with Applications*, Thomson Brooks/Cole, Belmont, CA, 2008.

[29] B. C. Gupta, I. Guttman, and K. Jayalath, *Statistics and Probability with Applications for Engineers and Scientists Using Minitab, R and JMP*, John Wiley & Sons, Inc, Hoboken, NJ, 2020.

[30] S. Jarrett, *The Effect of Bit Depth on High Temperature Digital Image Correlation Measurements*, Utah State University, 2021.

[31] Y. Q. Wang, M. A. Sutton, H. A. Bruck, and H. W. Schreier, "Quantitative error assessment in pattern matching: effects of intensity pattern noise, interpolation, strain and image contrast on motion measurements," *Strain*, vol. 45, no. 2, pp. 160–178, 2009.

[32] *Fine Extruded Graphite Rod, 0.5"OD × 12"L*, GraphiteStore, https://www.graphitestore.com/fine-extruded-graphite-rod-0-5od-x-12l-NNNNN001325.

[33] P. Reu, "All about speckles: contrast," *Experimental Techniques*, vol. 39, no. 1, pp. 1-2, 2015.

[34] H. Haddadi and S. Belhabib, "Use of rigid-body motion for the investigation and estimation of the measurement errors related to digital image correlation technique," *Optics and Lasers in Engineering*, vol. 46, no. 2, pp. 185–196, 2008.

[35] S. S. Fayad, D. T. Seidl, and P. L. Reu, "Correction to: Spatial DIC errors due to pattern-induced bias and grey level discretization," *Experimental Mechanics*, vol. 60, no. 4, p. 573, 2020.

[36] T. Archer, P. Beauchêne, C. Huchette, and F. Hild, "Global digital image correlation up to very high temperatures with grey level corrections," *Measurement Science and Technology*, vol. 31, no. 2, article 024003, 2020.